Spatial analysis of dead pixels

Julia Brettschneider, John Thornby, Tom E Nichols, Wilfrid S Kendall

Abstract

Considering a rectangular panel of pixels arranged in a grid, we introduce a taxonomy of damages based on spatial arrangements of dysfunctional pixels. We detect these different types of damage in experimental data obtained from a detector from an X-ray machine used for additive layer manufacturing object visualisation. We model the spatial distribution of dysfunctional pixels using point pattern analysis including intensity estimation and checking for CSR. As a practical application, we propose a protocol for performance monitoring for detector panels.

1 Introduction

Digital flat detector panels are used, for example, in computed tomography. Introductory references about this application are [4] and [2] The signals are detected by pixels arranged in a rectangular grid. With time of usage, some pixels become dysfunctional compromising the quality of the resulting images. Eventually, the detector needs to be refurbished or replaced at high cost. The aim of this study is to shed light on the kinds of dysfunctionality occurring in detector pixels and to model their spatial distribution.

The first task consists in providing a rigorous statistical definition for pixel behaviour that should be considered as dysfunctional. The panel manufacturer *PerkinElmer* has provided a set of criteria to identify what they call *underperforming pixels*. X-ray machines manufactured by *Nikon* (at their site at Tring, UK) include a protocol to create a *bad pixel map,* which actually consists of a collection of a number of test images and their statistical summaries as well as a list of bad pixel locations determined by the an evaluation of the images. We review these routines and conventions in Section 2.

We then analyse a collection of bad pixel maps taken on the same detector over a period of seven months (see Section 2). An initial round of exploratory data analysis in Section 3 sheds light on the different types of dysfunctionality that can be encountered for pixels and it guides our choice of spatial models in Section 4. Practical applications are discussed in Section 7. In the concluding Section 6 we discuss the findings and suggest future work.

2 Technology, conventions and data

The data used in this paper was collected with the XRD 1621 detector manufactured by *PerkinElmer* for use in X-ray machines. As detailed in the manual [6], it consists of a sensor and its electronics, with the latter placed on the perimeter of the active sensor, out of direct path of the beam. The user needs to block the radiation by lead shielding to avoid damage of the electronics and to adjust the *field of view (FOV).* The flat panel sensor of the detector is fabricated using thin film technology based on amorphous silicon

technology which detects visible light. The incident X-rays are converted by the scintillator material to visible light which generates electron hole pairs in the biased photodiode. The charge carriers are stored in the capacity of the photodiode. By pulsing the gates of a TFT line within the matrix, the charges of all columns are transferred in parallel to the signal outputs.

The detector is divided into two rows of 16 subpanels each, also called *read out groups (ROG),* divided by a midline. The upper and lower part are electrically separated. The data stream is detailed in Figure 1.

data stream no.	sensor pixel (row, column)	ROG no.
1	(1,1)	1
2	(1,129)	2
3	(1,257)	3
4	(1,385)	4
5	(1,513)	5
6	...	
15	(1,1793)	15
16	(1,1921)	16
17	(2048, 128)	18
18	(2048, 256)	17
19	(2048, 384)	20
20	(2048, 512)	19
...	...	...

Figure 1: **Sorting scheme of the XRD 1621 detector.** Each read out group has 128 channels for the detector. The upper groups scan the sensor columns from left to right. The lower groups scan from right to left. The upper groups are transferred first. The upper groups start read out from the upper row. The lower groups start read out from the last row.

In the literature, dysfunctional pixels are referred to by many names including *bad, dead, erratic, stuck, hot, defective, broken and underperforming,* and a variety of conceptions is associated with them.

Let n_1 and n_2 be the number of pixels in the horizontal and the vertical directions, respectively. An image taken by the detector in a fixed time point is denoted by $Z = (Z_i)_{i\in I}$, where Z_i is the value of the pixel i in the grid $I = [1,\dots,n_2] \times [1,\dots,n_2]$. Let $\overline{Z} = \text{median}\{Z_i | \, i \in I\}$ be the median of the pixel values across the whole grid and $\sigma(Z) = \text{SD}\{Z_i | \, i \in I\}$ be their SD.

For a sequence $(Z_i(j))_{i\in I}$ $(j = 1,\dots,m)$ of m such images we define, pixel wise, the *median image* and the *SD image*:

$$\overline{Z}_i = \text{median}\{Z_i(j) | \, j = 1,\dots,m\} \qquad (i \in I), \tag{1}$$

$$\sigma(Z)_i = \text{SD}\{X_i(j) | \, j = 1,\dots,m\} \qquad (i \in I). \tag{2}$$

We define summaries of these images across the whole grid: $\overline{\overline{Z}} = \text{median}\{\overline{Z}_i | \, i \in I\}$ is the median of the median image, $\sigma(\overline{Z}) = \text{SD}\{\overline{Z}_i | \, i \in I\}$ is the SD of the median image, and $\overline{\sigma} = \text{median}\{\sigma(Z)_i | \, i \in I\}$ is the median of the SD image.

The detector manufacturer *PerkinElmer* performs a final quality test and creates an *underperforming pixel map* to be delivered with the detector. They use a number of criteria to classify a pixel as *underperforming* based on signal intensities, noise levels, uniformity and lag. We summarise the criteria below and refer to the detector manual [6] for further details.

All tests are accomplished in the Timing 0 ($133.2\,ms$; ES: $T_0 = 66.6\,ms$), $200\mu m$ and at $1\,pF$ capacity, unless otherwise indicated. The bright image has a nominal value of roughly 30,000 units.

Signal sensitivity: Three types of underperforming pixels are detected through unusual response in a bright offset corrected image at three different X-ray energies at first free running timing.

- *Underperforming bright pixel:* value is greater than 150% of the median bright
- *No gain pixel:* dark pixel with no light response
- *Underperforming dark pixel*: value is below 45% of the median bright

Bright noise: A sequence $(X_i(j))_{i\in I}(j = 1, \ldots, m)$ of $m = 100$ bright images in the first free running timing T_0 is acquired. Pixel i is called *underperforming bright noise pixel* if $\sigma(Z)_i > 6\,\overline{\sigma}$.

Dark noise: A sequence $(Z_i(j))_{i\in I}(j = 1, \ldots, m)$ of $m = 100$ dark images in two free running timings T_0 and T_1 is acquired. Pixel i is called *underperforming dark noise pixel* if $\sigma(Z)_i > 6\,\overline{\sigma}$.

Uniformity: These criteria address maximum allowed deviations from overall means and from nearest neighbours. Let $(Z_i)_{i\in I}$ be an image acquired at T_0, corrected with gain? and offset? images also acquired at T_0. Pixel i is called *underperforming (with respect to global uniformity),* if

$$Z_i/\overline{Z} > 1.02 \qquad \text{OR} \qquad Z_i/\overline{Z} < 0.98. \tag{3}$$

Pixel i is called *underperforming (with respect to local uniformity),* if

$$Z_i/X_{i_{3\times3}} > 1.01 \qquad \text{OR} \qquad Z_i/Z_{i_{3\times3}} < 0.99. \tag{4}$$

Lag: The detector is set to an integration time of $2\,s$ (*triggered mode*). Three offset corrected frames are acquired: Image $Z^{(1)}$ is irradiated during the gap after the readout time of the detector of up to $30,000\,units$, and $Z^{(2)}$ and $Z^{(3)}$ are the following two dark images (first frame after exposure and second frame after exposure). A pixel i is marked as *underperforming,* if

$$Z_i^{(2)}/Z_i^{(1)} > \alpha_1 \qquad \text{OR} \qquad Z_i^{(3)}/Z_i^{(1)} > \alpha_2 \tag{5}$$

with thresholds $\alpha_1 = 0.08$ and $\alpha_1 = 0.04$ in the standard option (or $\alpha_1 = 0.1$ and $\alpha_1 = 0.05$ in the CsI option).

For detectors built into their X-ray machines, *Nikon* uses a monitoring protocol to create bad pixel maps. Each bad pixel map actually consists of a collection of ten data files:

1. mean white image containing the pixel wise means of the intensities of 100 white acquisitions, as well as images of the corresponding SDs, minima and maxima,
2. mean black image containing the pixel wise means of the intensities of 100 black acquisitions, as well as images of the corresponding SDs, minima and maxima,
3. a mean grey image containing the pixel wise means of the intensities of 100 images acquisitions (standard deviations, minima and maxima are *not* included),
4. list of bad pixel locations stored in an `.xlm` file.

Bad pixel maps in X-ray machines are routinely taken after a new detector is installed or an old one is reinstalled after refurbishment. Operators also have the option to take them at times of their convenience. In practice, they usually do so if they feel there "may be something wrong" with the detector.

The data set analysed in this paper comes from a collection of ten bad pixel maps taken between June 2013 and January 2014 on a X-ray machine with a *PerkinElmer* digital X-Ray Detector XRD 1621 AN/CN by the Warwick Manufacturing Group. Our analysis is based on the first six acquisitions, because the last four contain binned pixels, which implies that some of the information is lost making them less interesting for the analysis. The detector was refurbished between the fourth and the fifth acquisition. For more details see Figure 2.

	Timestamp	WhiteX	WhiteY	GreyX	GreyY	BlackX	BlackY
A_0	2013-06-13 13.31.51	2000	2000	2000	2000	2000	2000
B_0	2013-07-01 11.49.29	2000	2000	2000	2000	2000	2000
C_0	2013-10-02 13.41.00	1600	2000	1600	2000	1600	2000
E_0	2013-11-22 10.54.30	1600	2000	1600	2000	1600	2000
F_0	2014-01-28 11.48.00	2000	2000	2000	2000	2000	2000
G_0	2014-01-28 15.14.02	2000	2000	2000	2000	2000	2000
A_1	2013-06-13 16.14.34	1000	1000	1000	1000	1000	1000
D_1	2013-10-15 09.29.43	800	1000	800	1000	800	1000
F_1	2014-01-28 11.58.23	1000	1000	1000	1000	1000	1000
G_1	2014-01-28 15.19.30	1000	1000	1000	1000	1000	1000

Figure 2: **Bad pixel maps.** Test data collected by Warwick Manufacturing Group 2013-14 including acquisition date and x and y coordinate dimensions for each of the three parts: white image, grey image and black image. The last four of them contain binned images, that is, pixels are merged in pairs resulting in smaller images. The dimensions vary as a result of the binning and also because the images were cropped after an excess of bad pixels was detected near the edges.

3 Exploratory data analysis of bad pixel maps

The most obvious artefact in many of the images are parallel lines of different lengths, one end meeting the midline at an orthogonal angle and the other end at what seems a random location somewhere in the grid on either side of the midline. Figure 3 shows a part of the grey image of A_0 displaying the phenomenon.

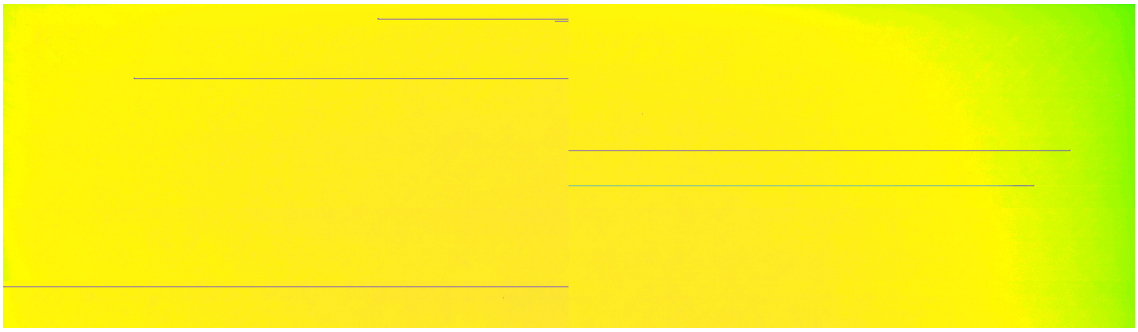

Figure 3: **Lines between clusters and midline.** Left part of grey image of A_0 shown after 90 degree anticlockwise rotation. Horizontal midline (shown here as vertical line) divides upper row (shown on the left) from lower row (shown on the right). It shows parallel lines connected to the midline from both sides. There is also visible inhomogeneity of intensity, with darker areas near the corners.

Our systematic assessment of the spatial locations of bad pixels is based on bad pixel lists. Our tool for this are *bad pixel images,* that is, an image created from the list of bad pixel coordinates (stored in an `.xml` file as part of the bad pixel map, see Section 2 for details) as coloured squares in their original location in a grid. As colour code we use beige for bad pixels and red for others. (Printed in grey scale, the bad pixels are displayed as bright on a dark background.)

3.1 A taxonomy for bad pixel arrangements

Visual inspection of all the bad pixel images in our data set revealed several types of spatial arrangements of bad pixels. We have classified them into six categories listed below. *Nearest neighbour* of a pixel refers to the pixels on the left, right, top or bottom of the pixel; the pixels touching it only at corners (diagonal) are not included. A *corner piece* consists of three neighbouring pixels that are not in a line.

1. *Singletons.* Individual bad pixels.
2. *Doubles.* Two neighbouring bad pixels.
3. *Small clusters.* Three or more neighbouring bad pixels including at least one corner piece.
4. *Lines to midline.* Three or more bad pixels arranged in a line leading up to the midline that divides the upper from the lower row of subpannels.
5. *High density regions.* Areas with visibly higher concentration of single bad pixels.
6. *Corner damage.* Massively damaged area in a corner amounting to connected areas of damage as shown in Figure 5.

The examples below illustrate these types. The bad pixel images areas shown in Figure 4 illustrate the first five types of spatial arrangements of bad pixels. Usually, small

clusters and lines occur together. However, there are instances of lines of bad pixels that are connected to the midline on one end, but do that do not end in a cluster on the other end (bottom left in Figure 4), and there are also instances of small clusters that are not connected to a line. Figure 5 shows the four corner areas of the bad pixel image for B_0, all heavily damaged.

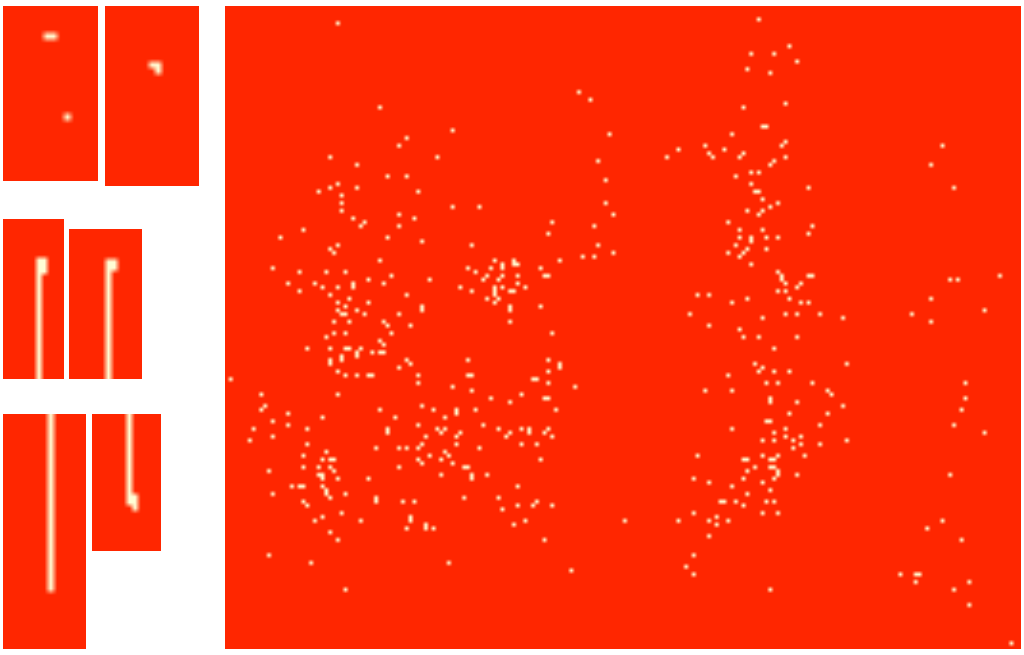

Figure 4: **Spatial arrangements of bad pixels.** Selected areas from bad pixel images A_0 to F_0. The two areas in the upper left row shows singletons, doubles and corner pieces. Three of the other four areas on the left show small clusters with consequent lines as well as one line with no cluster. The big area on the right is a region of high density of bad pixels.

The black and white plots in Figure 6 show the locations of bad pixels for the six regular bad pixel maps in our data set (not the binned ones). There are many dysfunctional lines going up and down from the midline in the first four images. After that, the detector was refurbished and the last two images demonstrate that most of the lines have now disappeared. However, both of these images have areas with high bad pixel intensity that were not present in previous images.

3.2 A closer look on dysfunctional lines

The acquisitions that produced the largest number of lines are C_0 and E_0 with 9 dysfunctional lines in the upper row of subpanels and 8 lines in the lower row. A_0 has 7 and 5 and B_0 has 7 and 8, usually in the same locations as C_0 and E_0, though length may vary. F_0 and G_0 were obtained after refurbishment of the panel and only have one line in the upper row and one line in the lower row.

All the lines are just one pixel wide. (Hence they can not be seen in the binned images A_1, D_1 , F_1 and G_1.) With one exception, one end of the line always reaches the

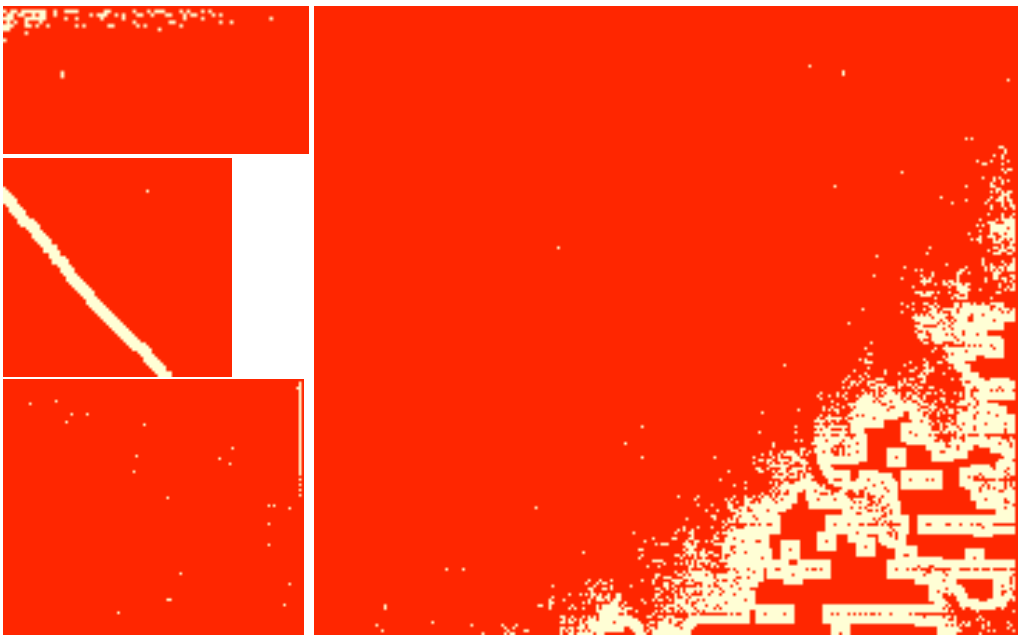

Figure 5: **Corner damage.** Corner areas of bad pixel images for B_0. All four corner areas are seriously damaged.

horizontal midline. The exception is a line in column 744 in F_0, which ends 4 pixels before it reaches the midline. For the other end there are three possibilities: ending in just one pixel, running all the way to the other side of the sub panel, or ending somewhere in a small cluster. The last two options are the most frequent ones. The clusters have some commonalities. Broadly speaking they are 1 to 3 doubled up bad pixels to the right of the line. To illustrate this in more detail, here is a list of the types of all the 17 non-midline ends in C_0 with their frequency

1. line ends in one pixel somewhere in the sub panel: 1
2. line runs to the other side of the sub panel: 4
3. line ends in a small cluster: 12, of which
    - endpoint of the line has another bad pixel adjacent to it on the right: 7
    - last two pixels of the line have bad pixels adjacent to it on the right: 4 (in one case there is an extra bad pixel to the left, too)
    - last three pixels of the line have bad pixels adjacent to it on the right: 1 (on top of that, there is an extra bad pixel above these adjacent pixels)

Andrew Ramsey from Nikon has suggested that the lines are not all themselves bad pixels. Instead, only the cluster consists of bad pixels, but they block the signal transmission of all subsequent pixels in the same line. The occurrence of lines connecting some a pixel located somewhere in a (sub-)panel with the border of a sub panel (here the midline) has also been documented in forums of the photography and astronomy community, under the term *hot pixel lines*: see for example

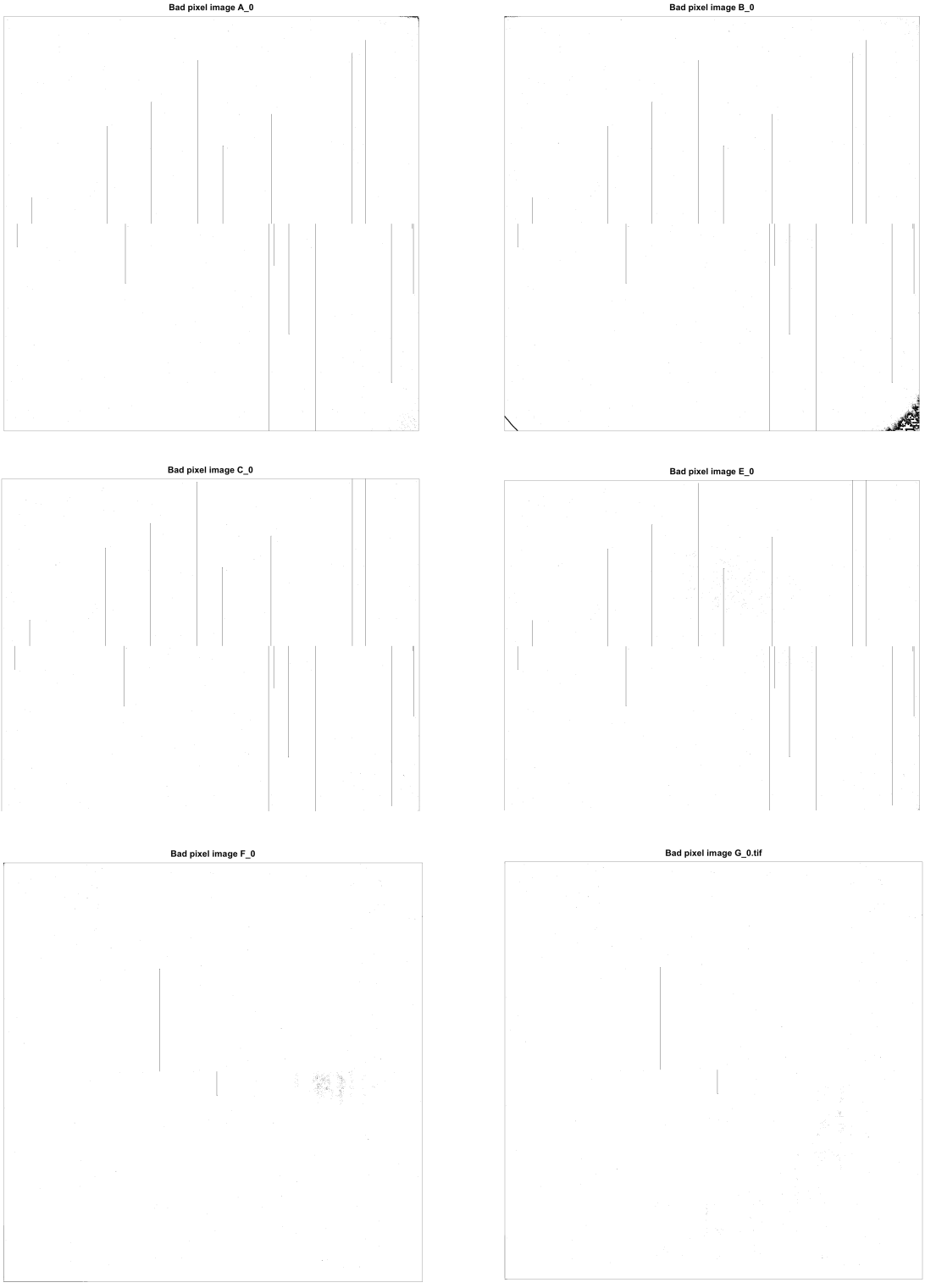

Figure 6: **Bad pixel images.** Bad pixels are plotted in black against white background. The image in the top row show very noticeable damage, especially in the regions close to the corners and edges. The middle row is taken after the image has been cropped. The acquisitions in the bottom row were taking after refurbishment of the detector.

`www.ls.eso.org/lasilla/Telescopes/3p6/efosc/docs/BADPIXMASK/Ccd40Cosmetics.html`,

`www.astro-wise.org/portal/howtos/man_howto_hot/man_howto_hot.shtml`.

It has been suggested that dysfunctional pixels destroy the value of all pixels behind the broken pixel as charge is moved through it during the read-out process. In the analysis of the lines, we will therefore focus on the locations and shapes of the endpoints rather than the modelling the occurrence of complete lines.

4 Spatial models and analysis

Our models for the spatial distribution of dysfunctional pixels is based on random point patterns. An overview of these models and methods can be found, for example, in [5] and [1], with the latter emphasising on R-implementation using packages such as `spatstat, sp` and dependencies. Once the data has been imported into a `ppp`-object, it is straight forward to plot images of the point pattern highlighting the events by out-of-scale plotting characters. Figure 7 shows such images of the detector before and after refurbishment.

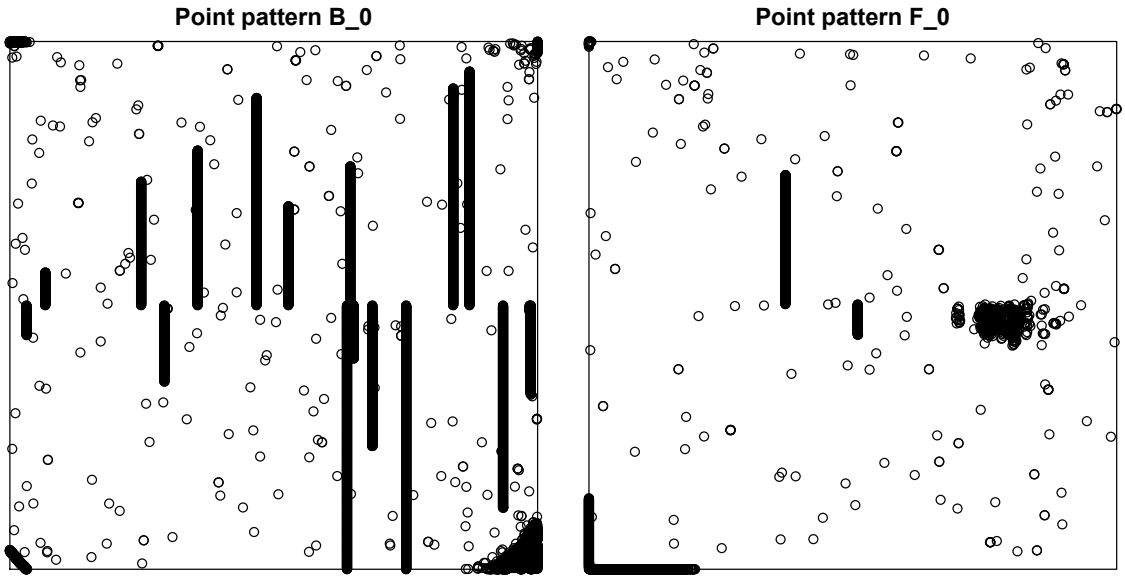

Figure 7: **Point patterns.** B_0 and F_0 straight from raw data showing the difference before and after refurbishment.

There are two perspectives leading to different mathematical descriptions of the detector and its dysfunctional pixels. In the previous sections, we recorded the state of the detector at one moment in time as a random field indexed by the two-dimensional grid $I = [1, \ldots, n_2] \times [1, \ldots, n_2]$. The values of the random field can be numeric to describe the actual value of the pixel or they can be binary indicating its dysfunctional versus functional status. The latter can also be extended to taking categorical values accounting for different types of dysfunctionality.

Consider now that our main interest is in the dysfunctional locations, with the rest of the panel acting as background only. The essential information can be represented as a

spatial point process X with values x_k in the rectangle $S = [0, n_2] \times [0, n_2]$, with finite total intensity. Points correspond to the event that the pixel centred there is dysfunctional. For any $A \subseteq S$, the number of points in A is denoted by $N(A)$, and $N = N(S)$ is the total number of points.

To build appropriate spatial point pattern models we briefly return to our taxonomy of damages from Section 3. We first exclude two of the damage types from modelling.

Firstly, we do not include the whole dysfunctional lines, but restrict ourselves to modelling the small clusters at the end far off the midline. (In the rare case where there is no cluster, we only use the endpoint.) This is necessary, because even very few short lines quickly dominate calculations testing for CSR making it impossible to detect what goes on in the rest of the image. This is illustrated by simulations in Figure 9, using the descriptive functional statistics known as G-, F-, and K-functions, described for example in [3]. The simulations show how sensitively these react to even just one or two short lines for point densities slightly higher than in our images. The effect on G and K is particularly sharp with obvious changes in $r = 1$ caused by the sudden huge increase in the number of adjacent bad pixels. It gets more pronounced for lower densities and less pronounced for higher densities; see Figures 14 and 15 in the appendix.

Secondly, the corner damages are rather peculiar and not well suitable for modelling. Since they are located at the margins of the images, restricting models to a cropped image is an appropriate strategy and reflects the common practice of reducing the FOV of the detectors after issue have been detected near the edges. C_0 and E_0 were already cropped by 200 rows both on top and bottom during acquisition. Based on visual inspection we cropped an additional 50 rows on these and accordingly cropped A_0 and B_0 by 250 rows both on top and bottom. The images acquired after refurbishment of the projector, F_0 and G_0, were cropped by 5 pixels all around to exclude artefacts on the edges. Figure 8 shows the point patterns after removal of lines and illustrates the relevance for cropping.

We now study fundamental properties of the spatial point patterns including complete spatial randomness (CSR), homogeneity and intensity estimation as described for example in [3].

The G-, F-, and K-Functions for our data have been calculated based on 100 Monte Carlo simulations under CSR. Default confidence intervals of 96% are used. For each of the images, the G-Function in Figure 10 indicates aggregation for short ranges, while they seem to behave more randomly at larger distances. A_0, B_0 and C_0 show a jump like increase in $r = 1$, but little further increase beyond. In contrast, E_0, F_0 and G_0 increase about equally strongly, but more smoothly for small r. This is most likely related to the existence of a small area of high density of bad pixels in the last three images, but not the first three. In turn, the deviations from CSR in the first three images are the result of an unusually high amount of doubles and very small clusters (see last column in Table 13). The behaviour of the F-Functions in Figure 11 confirms this, with aggregation particularly pronounced in the last two images.

The normed K-Functions in Figure 12 give the same picture. There is strong evidence for aggregation with respect to small distances, especially very ones. For images A_0, B_0 and C_0 this almost exclusively driven by $r = 1$, in other words, by adjacent bad pixels. They correspond to doubles and small clusters. In fact, between 12.6% and 14.9% of the pixels locations are actually of this kind (see Figure 13.) In images E_0, F_0 and G_0 there

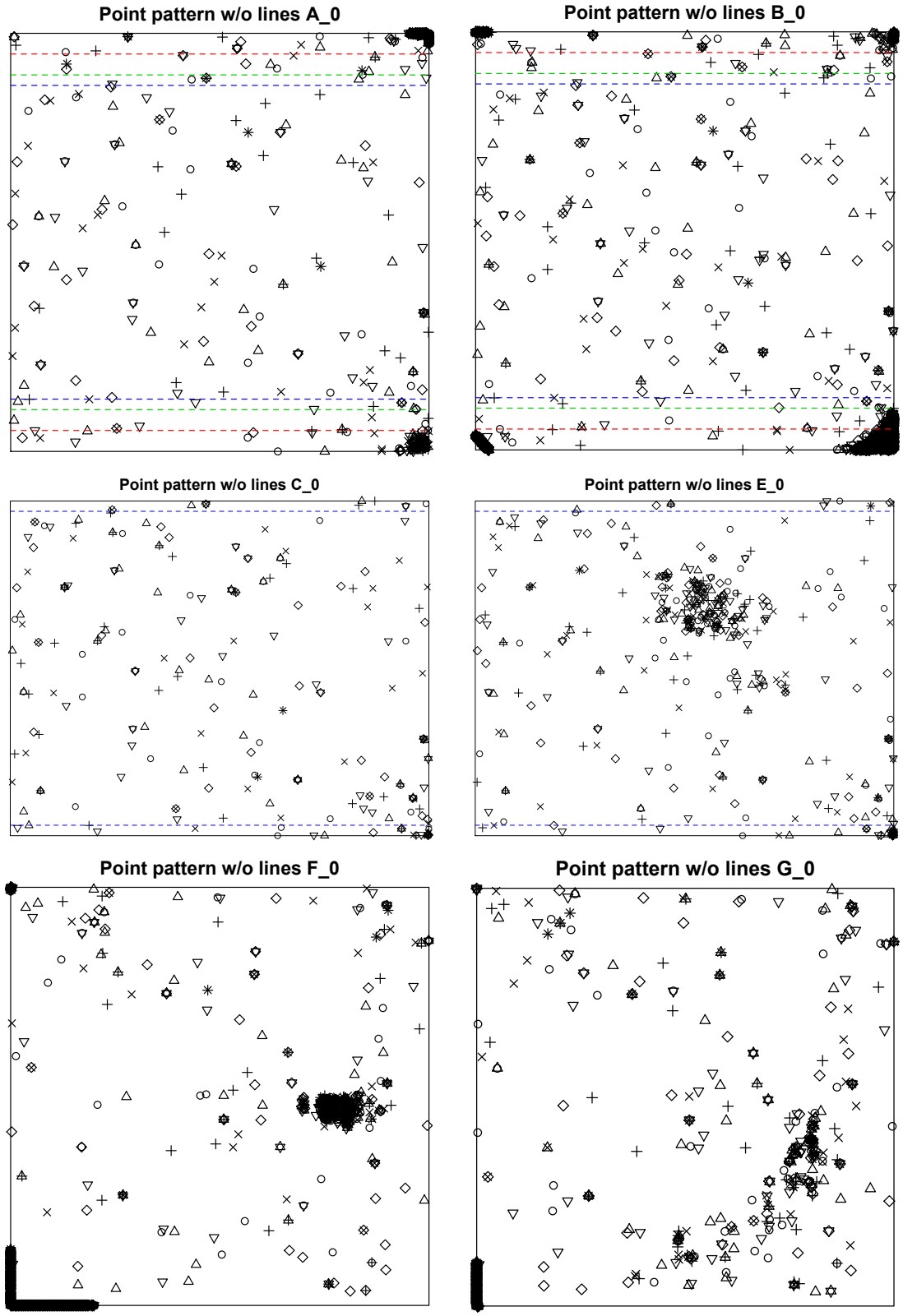

Figure 8: **Point patterns without lines.** Defective pixels in first six images after removal of dysfunctional lines except their outer end points. Plotting characters are randomly assigned to better distinguish points in close proximity and they are bigger than the original pixels. A_0 and B_0 are marked with horizontal lines indicating potential cropping of the image at y coordinates 100 and 1900 (red), or 200 and 1800 (green), or 250 and 1750 (blue). All four corner areas are seriously damaged. C_0 and E_0 are already cropped by 200 on both top and bottom, and we indicate cropping by an additional 50 more rows on both top and bottom by the blue line.

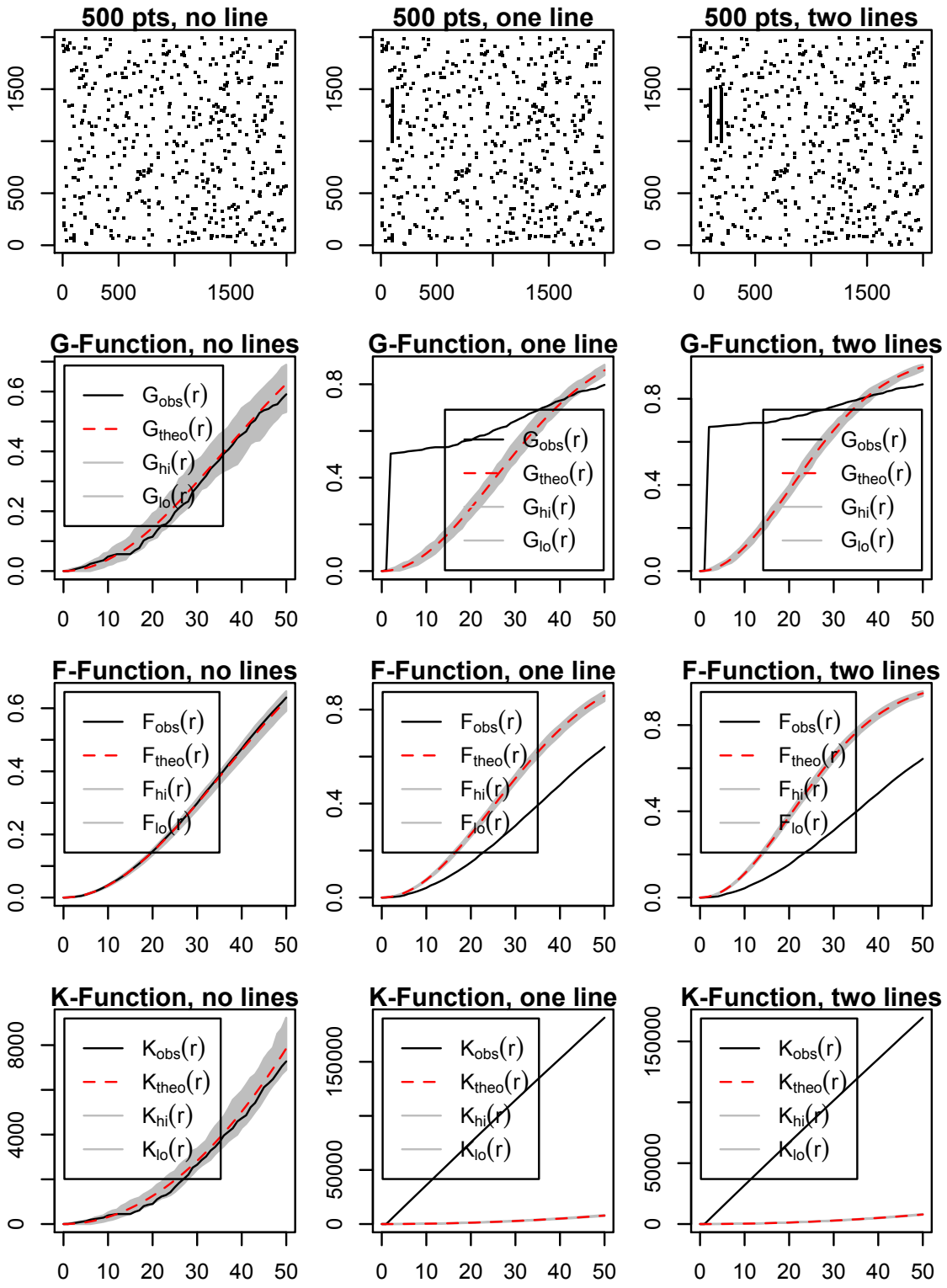

Figure 9: **Sensitivity to lines.** Simulations of random scatters of 1000 points (medium intensity) on a 2000 x 2000 grid with no, one or two lines of length 500 added to it. G-, F-, and K-Function estimates are calculated based on 49 CSR simulations. Scales on x-axes are standardised across images, but scales on y-axes are not.

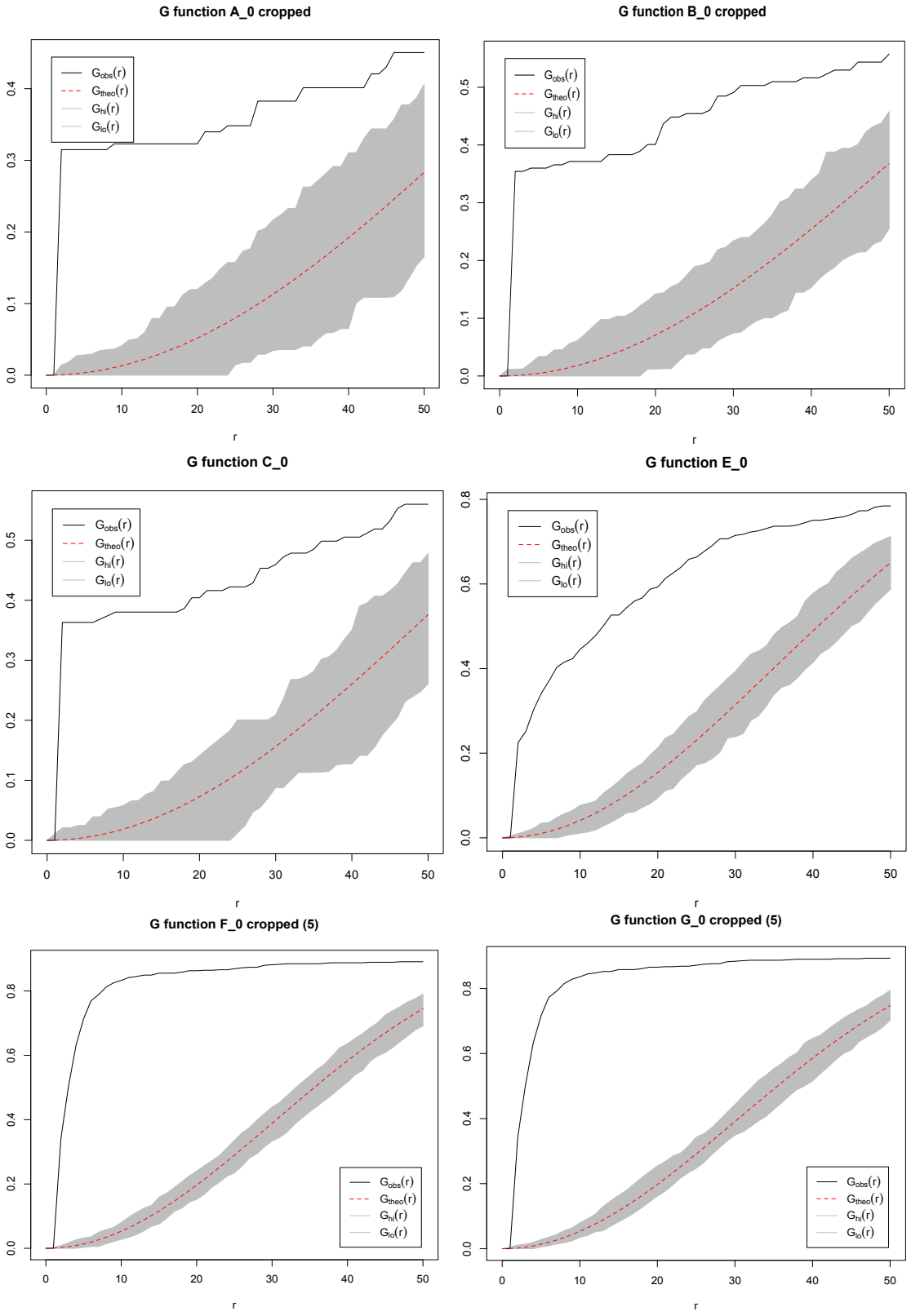

Figure 10: **G-Function.** G-Functions for all images (suitably cropped as described above) with upper and lower confidence bounds bordering the grey area. Scales on x-axes are standardised across images, but scales on y-axes are not.

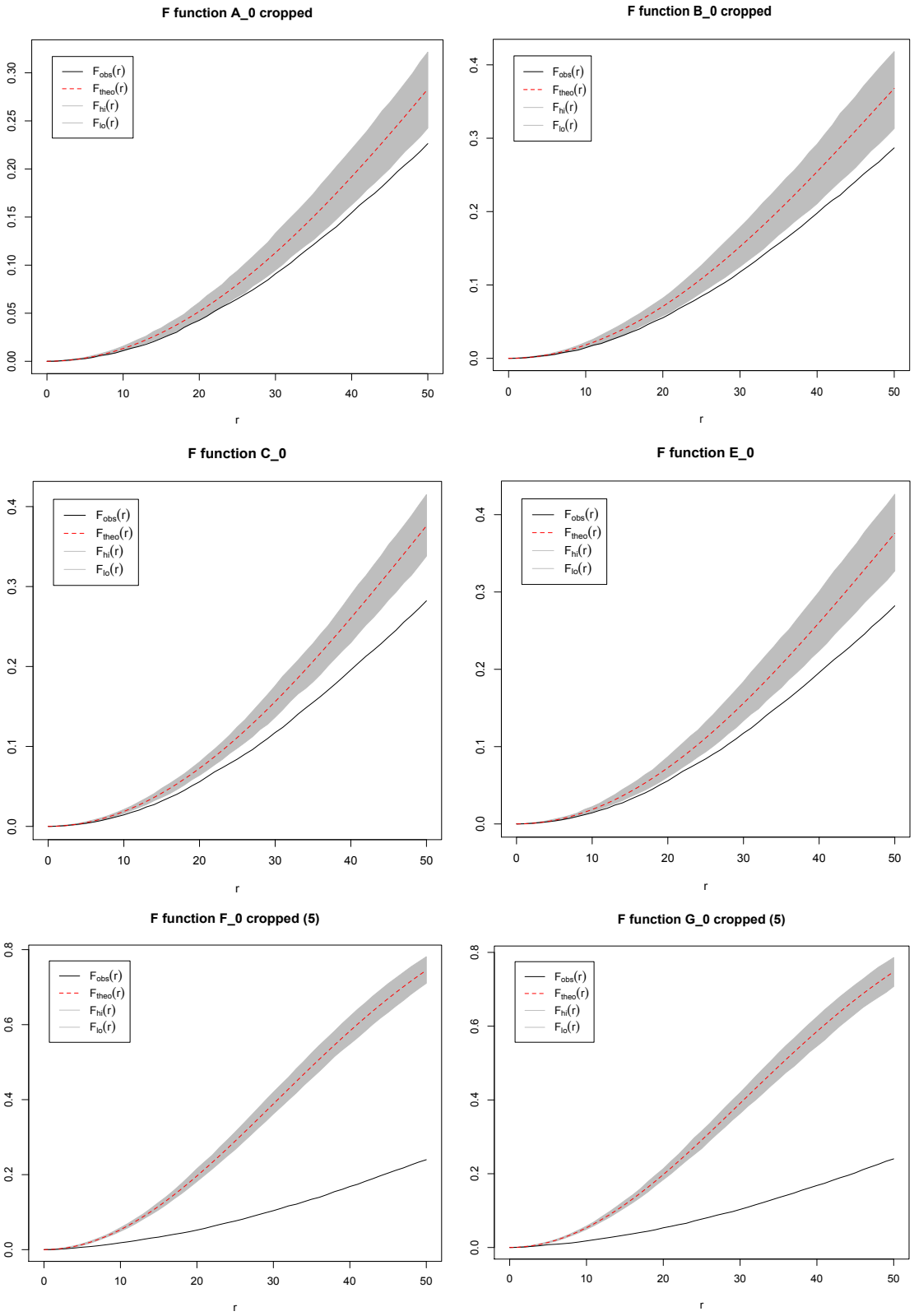

Figure 11: **F-Function.** F-Functions for all images (suitably cropped as described above) with upper and lower confidence bounds bordering the grey area. Scales on x-axes are standardised across images, but scales on y-axes are not.

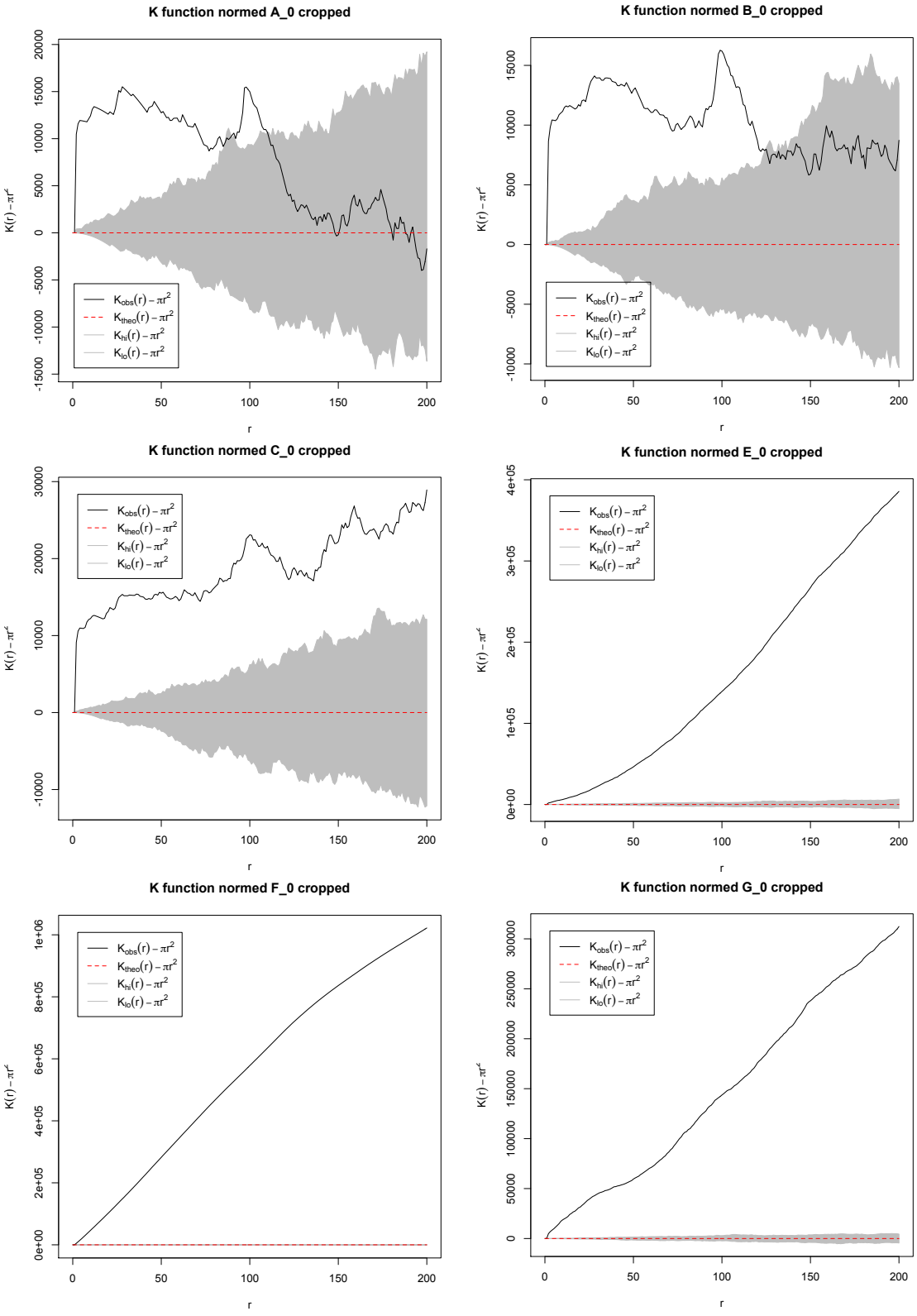

Figure 12: **K-Function.** K-Functions for all images (suitably cropped as described above) with upper and lower confidence bounds bordering the grey area. Scales on x-axes are standardised across images, but scales on y-axes are not.

are additional small range interactions from the areas with increased density of bad pixels (see Figure 8).

The observed intensities are summarised in Table 13. The assumption of homogeneity seems suitable for the first four images (after suitable cropping of corners and edges). For the last two images a homogeneity assumption seems wrong, given each of them has a quite well defined area with an strongly increased density of bad pixels. The obvious alternative is to consider inhomogeneous models. However, the areas of high intensity of bad pixels may be the result of somewhat arbitrary cut-offs in the definition of bad pixels. A sensitivity analysis based on varying these cut-offs is recommended.

	Areas	Number of bad pixels	Intensities	Small clusters in selected area
A_0	[0,2000]x[0,2000] [0,2000]x[250,1750]	625 127	15.625 4.233	NA 16 [12.6%]
B_0	[0,2000]x[0,2000] [0,2000]x[250,1750]	7053 175	176.325 5.833	NA 26 [14.9%]
C_0	[0,2000]x[0,1600] [0,2000]x[250,1750]	219 180	6.843 6.000	NA 25 [13.9%]
E_0	[0,2000]x[0,1600] [0,2000]x[250,1750]	427 362	13.344 12.067	NA 21 [5.8%]
F_0	[0,2000]x[0,2000] [5,1995]x[5,1995]	1412 694	35.300 17.437	NA 31 [4.5%]
G_0	[0,2000]x[0,2000] [5,1995]x[5,1995]	576 352	14.400 8.844	NA 31 [8.8%]

Figure 13: **Bad pixel counts and intensities.** For each image, bad pixel counts for both original image and suitably cropped image (as explained above) are given and corresponding intensities (multiplied with the factor 100,000) under homogeneity assumption. The last column shows the number of doubles. (For E_0 and G_0 the counts of doubles exclude the areas of high intensity of bad pixels.

5 Applications to detector performance monitoring

Based on the models introduced in the last section we suggest the following basic protocol for detector performance monitoring. The emphasis of the protocol is on the spatial distribution of dysfunctional pixels. This protocol can be used to establish benchmarks for detector performance, more specifically, for objectives including the following:

- Determining sufficiently functional FOV;
- Determining need for refurbishment;
- Comparing performance of different types of detectors;

- Detecting performance differences between subpanels;
- Linking defects to problems in the detector manufacturing process or usage.

The protocol can be carried out employing some of the diagnostic tools used in the previous sections. The starting point for the analysis is the list of bad pixel locations.

1. **View.** Visualise the location of the bad pixels by plotting them in their original locations in a square. *Diagnostic tools:* Plots as in Figure 7 give a quick impression.
2. **Classify.** Make a frequency table of all types of spatial arrangements of bad pixels in the data set. This is to confirm whether the panel has the types of defects known from previously studied panels and potentially adds new types to the list. *Diagnostic tools:* Plots as in Figure 6 are suited to view details. It may be necessary to zoom in, because individual pixels are very small.
3. **Crop.** Based on visual inspection using the plots from the first two steps, reduce image by cropping marginal rows and/or columns as appropriate, to exclude corner or edge issues currently not addressed by modelling.
4. **Model.** Fit a spatial point pattern model.
   (a) If lines occur in the bad pixel map image, keep only the endpoint far the middle line in the bad pixel list.
   (b) Examine whether the remaining pattern is *random* in the sense of complete spatial randomness (CSR). If it is not random, determine whether there may be regularity or aggregation. Determine which point distances drive these behaviours. *Diagnostic tools:* Study the graphs of the G-, F- and K-Functions, as shown in Figures 10, 11 and 12.
   (c) Estimate the intensity under homogeneity assumptions, as appropriate. Otherwise consider fitting a heterogeneous density. However, since the definition of bad pixel is based on thresholds and the scanning has been performed under not necessarily universal parameters, back this up with sensitivity analysis.
5. **Subpanels.** Perform the model fit sketched above separately for the different subpanels. Check whether there are systematic differences between the subpanel that could potentially be linked to the manufacturing process or modes of usage. *Diagnostic tools:* As in previous steps. In addition, plot of the bad pixel locations on the panel can be overlaid with a grid showing the subpanel division for visual examination of subpanel related artefact. A χ^2-test for independence can be performed on the counts of bad pixels on the subpanels.

6 Discussion, conclusions and future work

The analysis in the report focusses on the spatial distribution of bad pixels as stored in the bad pixel list of flat screen X-ray detectors. It is based on a series of *bad pixel maps* collected before and after a refurbishment of a detector. Informed by an initial step of exploratory data analysis the test images, we propose a taxonomy for pixel damage by

their spatial arrangements: Singletons, doubles, small clusters, high density patches, lines and corner damage.

The last two types of damages are treated differently than the others. Corner damages are related to known physical causes such as increased stress related to mounting and more rigidity of the material closer to the corners. The damage caused by them can be controlled by adjusting the FOV of the detector. We therefore exclude corner damages from the modelling. Dysfunctional lines can start in any location and, with the notable exception of one in this data set, end at the midline. The most common explanation is that they are the result of a data stream interruption due to a single or, more typically, small cluster of bad pixels on one end. We therefore restrict the spatial analysis to the non-midline endpoints of the dead lines.

The occurrence of singletons, doubles and small clusters of bad pixels has been studied using models for spatial point patterns. Using G-, F- and K-functions, we found that all the six images deviate from the CSR assumption due to aggregation on small ranges, even very ones. There are two obvious potential reasons for these deviation, and it is likely that what remains after their removal would actually fulfil the CSR assumptions.

The first reason are small areas of high density as found in E_0, F_0 and G_0. They could be excluded from the model like the corners. Or they could be modelled using non-homogeneous processes. However, they typically have quite clear boundaries potentially leading to an intensity function with high gradients.

The second reason are unusually high numbers of doubles and very small clusters that are not matched by comparable aggregation at bigger ranges. The unexpected frequency of doubles and small clusters was one of the bigger surprises in this data analysis. Asking for the reason brings us back to the original set-up of the spatial point pattern model. In our models, we have identified points with the event that an individual grid pixel is dysfunctional. It can be argued, though, that the elementary event of interest is a kind of damage that can extend to one, two or a small cluster of pixels as part of the *same mathematical event*. This is a very intuitive approach for the scenario where damage is caused by an external force that may hit the panel in a small location covering some amount of pixels up to a small cluster. Hence, an alternative set-up for the spatial point process models would be to identify points with dysfunctional locations of the size up to small clusters counting them as one only.

Translating this intuition into a formal model has to overcome two hurdles. Firstly, the definition of what a small cluster is, as opposed to say several adjacent clusters or a small region of high density, will remain somewhat arbitrary. Secondly, clusters may contain pixels with different types of dysfunctionality, making it complicated to assign a mark for the points representing these events.

Furthermore, our perspective is blind to the original arrangement of the pixels in a grid. There, the vertical and the horizontal direction are distinguished, reflecting the physical structure of the panel. Another investigation would be to pay special attention to the behaviour along both of these directions. In other words, the spatial point process perspective could be supplemented by one-dimensional analysis.

Labelling a pixel as *bad* is not absolute. The classification depends on scanning parameters set during the acquisition of the image and on thresholds in the definitions used

to create the bad pixel map. The more characteristic damages at the corners and edges, and the isolated singleton, doubles and small clusters, may persist independent of these settings. However, it has been suggested by users that some of the patches with high bad pixels density are sensitive to these settings.

We have focused on spatial arrangement of pixels classified as *bad* according to the bad pixel map protocol of the kind used by *Nikon.* Future work should extend the current discussing including also the temporal evolution of pixel dysfunctionality. A collection of test images taken at regular intervals over an extended period of time should be assembled. An initial step of temporal modelling includes determining potential stages until a pixel is fully *dead,* analyse how long pixels typically stay in these stages and find out whether they can move between them. Combining this with results from spatial analysis, spatio-temporal models for pixel damage should be fitted.

In terms of the models used, different types of dysfunctionality can be accounted for by extending this set-up to a marked spatial point process. For example, marks could be assigned to distinguish ends of lines from isolated small damages, or to label pixels according to different criteria for underperformance listed in Section 2.

The methods presented here have practical applications to the monitoring, refurbishment and manufacturing of detectors. A toolbox of statistical techniques is presented and can be put to use as needed by users of the detectors. For example, comparing the damage intensity across subpanels determines whether some of them need to be exchanged. Spatial patterns of bad pixels may give clues to the causes of the damage related to either the manufacturing or the time or modes of use.

Acknowledgements

The authors wish to acknowledge funding by EPSRC grant EP/K031066/1.

References

[1] Roger S Bivand, Edzer J Pebesma, and Virgilio Gómez-Rubio. *Applied spatial data analysis with R*, volume 747248717. Springer, 2008.

[2] Angela Cantatore and Pavel Müller. Introduction to computed tomography. Technical report, DTU Mechanical Engineering, 2011.

[3] Sung Nok Chiu, Dietrich Stoyan, Wilfrid Stephen Kendall, and Joseph Mecke. *Stochastic Geometry and Its Applications*. John Wiley and Sons, June 2013.

[4] Maire E. and Withers P. J. Quantitative X-ray tomography. *International Materials Reviews*, 59(1):1–43, 2013.

[5] Carlo Gaetan, Xavier Guyon, and Kevin Bleakley. *Spatial statistics and modeling*, volume 271. Springer, 2010.

[6] PerkinElmer. Reference Manual Digital Imaging, XRD 1621 AN/CN Digital X-Ray Detector.

7 Appendix

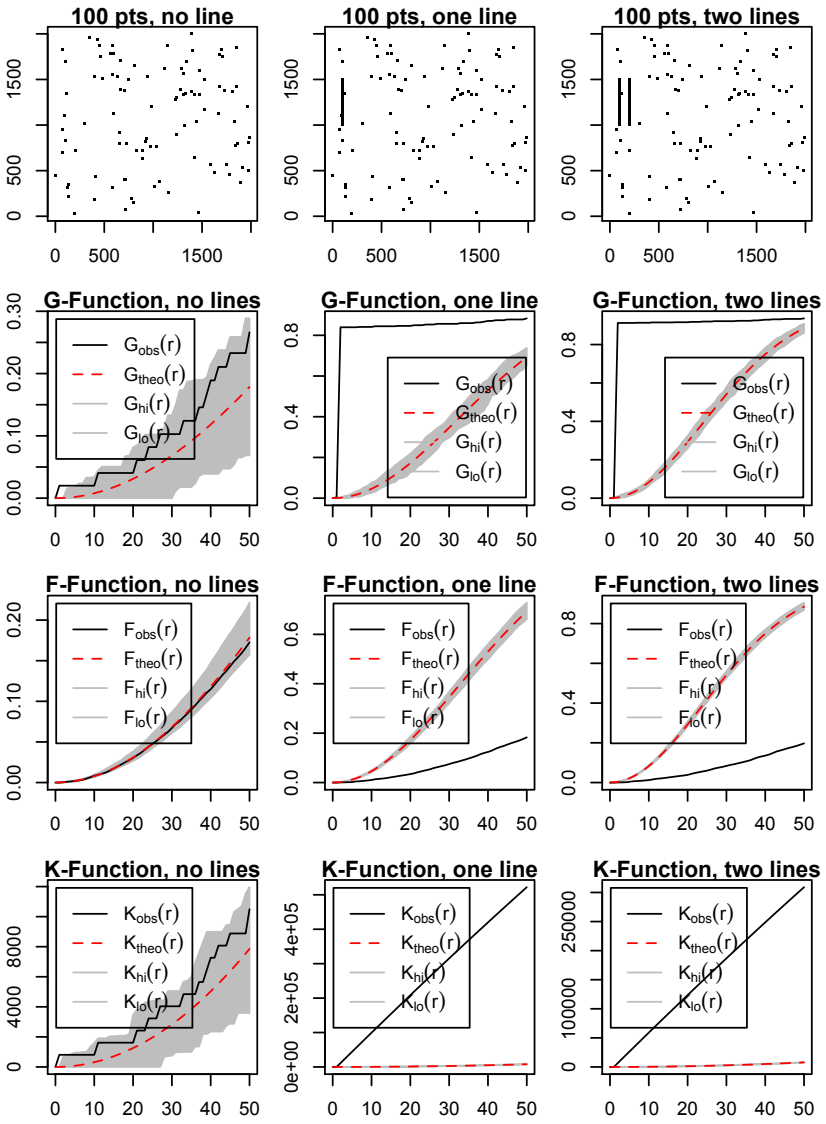

Figure 14: **Sensitivity to lines.** Simulations of random scatters of 100 points (low intensity) on a 2000 x 2000 grid with no, one or two lines of length 500 added to it. The G-, F-, and K-Function estimates are calculated based on 49 CSR simulations. Scales on x-axis are standardised across images, but scales on y-axis are not.

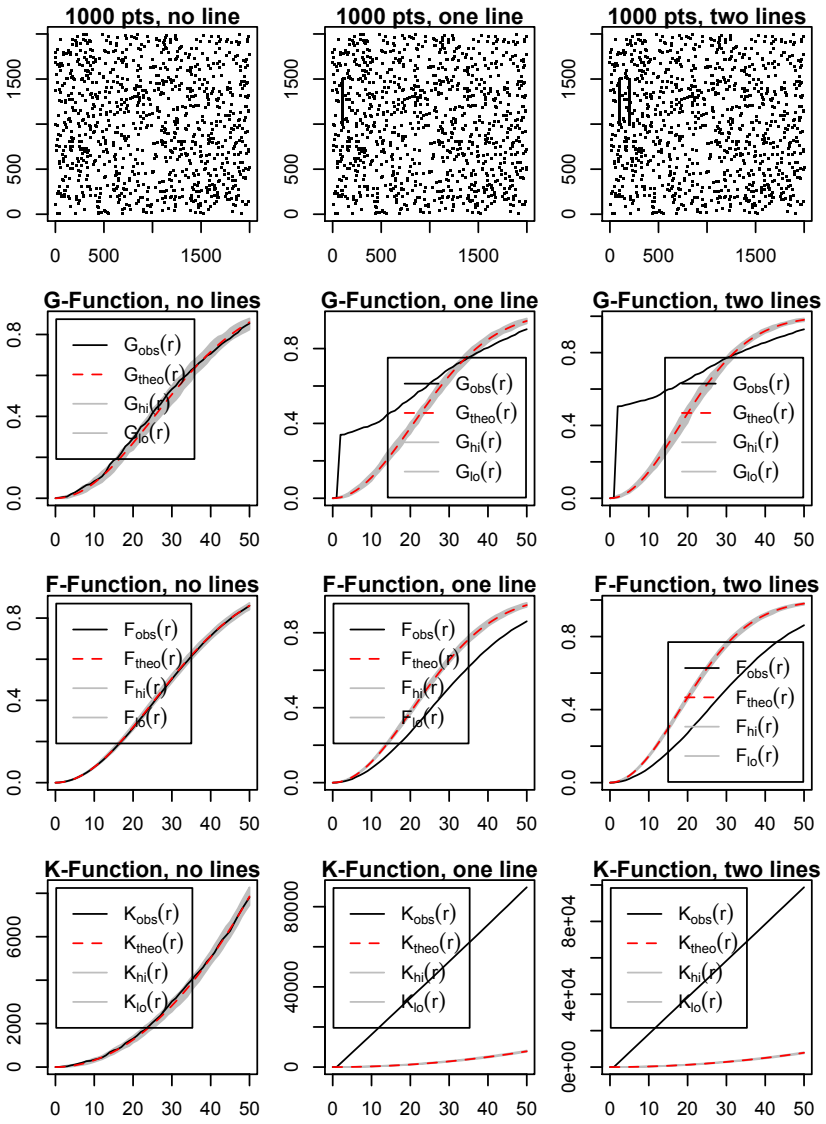

Figure 15: **Sensitivity to lines.** Simulations of random scatters of 1000 points (high intensity) on a 2000 x 2000 grid with no, one or two lines of length 500 added to it. The G-, F-, and K-Function estimates are calculated based on 39 CSR simulations. Scales on x-axis are standardised across images, but scales on y-axis are not.